HHS Public Access

Author manuscript

Nat Immunol. Author manuscript; available in PMC 2018 April 23.

Published in final edited form as:

Nat Immunol. 2017 December ; 18(12): 1353–1360. doi:10.1038/ni.3866.

Directing leukocyte polarization and migration by the phosphoinositide transfer protein TIPE2

Svetlana A. Fayngerts[1,3], **Zhaojun Wang**[1,2,3], **Ali Zamani**[1], **Honghong Sun**[1], **Amanda E. Boggs**[1], **Thomas P. Porturas**[1], **Weidong Xie**[1], **Mei Lin**[1], **Terry Cathopoulis**[1], **Jason R. Goldsmith**[1], **Anastassios Vourekas**[1], and **Youhai H. Chen**[1,4]

[1]Department of Pathology and Laboratory Medicine, Perelman School of Medicine, University of Pennsylvania, Philadelphia, PA 19104, USA

[2]Department of Immunology and Microbiology, School of Medicine, Shanghai Jiao Tong University, Shanghai 200025, China

Abstract

Leukocyte polarization toward chemoattractants is essential for directed leukocyte migration, or chemotaxis. How leukocytes acquire polarity upon encountering chemical gradients is not well understood. We report here that leukocyte polarity is generated by TIPE2 (TNFAIP8L2), a transfer protein of phosphoinositide second messengers. TIPE2 functioned as a local enhancer of phosphoinositide-dependent signaling and cytoskeleton remodeling, promoting leading edge formation. Conversely, TIPE2 acted as an inhibitor of the GTPase Rac, promoting trailing edge polarization. Consequently, TIPE2-deficient leukocytes were defective in polarization and chemotaxis, and TIPE2-deficient mice were resistant to leukocyte-mediated neural inflammation. Thus, the leukocyte polarizer is a dual-role phosphoinositide transfer protein, and a potential therapeutic target for treating inflammatory diseases.

Introduction

Leukocytes, like all eukaryotic cells, sense the presence of chemical attractants (chemoattractants) mostly through chemotactic receptors of the G protein-coupled receptor (GPCR) family. Upon binding to chemoattractants, GPCRs activate several intracellular signaling cascades via their associated G proteins, which lead to a marked morphological and biochemical transformation called polarization[1]. The front pole, or the leading edge, of a

[4]Correspondence should be addressed to Y.H.C. (yhc@pennmedicine.upenn.edu).
[3]These two authors contributed equally to this work

Note: Supplementary Information is available in the online version of the paper.

Author Contributions

S.A.F. and Z.W. conceived and Y.H.C. supervised this study. S.A.F. and Y.H.C. wrote the article. S.A.F. designed and performed the experiments and analyzed the data. Z.W. designed and performed the *in vivo* experiments. A.Z., A.E.B., T.P.P., W.X., M.L., T.C., J.R.G and A.V. were involved in the design or execution of several experiments. H.S. bred mice and performed μ–slide migration assay.

Competing financial interests

The authors have no financial conflict of interest with this work.

polarized leukocyte is characterized by dynamic actin remodeling that generates the protrusive structure and the forward-moving force. The rear pole, or the trailing edge, possesses only a limited amount of stable filamentous actin (F-actin or polymerized actin) that facilitates myosin-dependent cell retraction. This morphological polarity is determined by asymmetrical activation of proteins such as phosphoinositide 3-kinases (PI(3)Ks), GTPase Rac, and actin regulatory proteins at the leading and trailing edges[1–3]. How GPCR-generated signals direct and steer cells along chemoattractant gradients (as shallow as 2%) is not well understood. Several computational models have been proposed to address this issue. It is predicted that both enhancers and inhibitors of signaling transduction and actin dynamics are required for leukocyte polarization and chemotaxis[1,4–6]. The enhancers operate locally at the leading edge, whereas the inhibitors function globally. However, the nature of these regulators remains to be characterized[1,4–6].

The mammalian TIPE [tumor necrosis factor-α-induced protein 8 (TNFAIP8)-like or TNFAIP8L] family consists of four proteins that include TNFAIP8, TIPE1 (TNFAIP8L1), TIPE2 (TNFAIP8L2), and TIPE3 (TNFAIP8L3). TIPE proteins are risk factors for both inflammation and cancer[7–9] and their expression is dysregulated in a number of human diseases[10–16]. They share a highly conserved TIPE2 homology (TH) domain, a barrel-like fold with a lipophilic central cavity[10,17]. Previously, we demonstrated that all TIPE proteins can bind phosphoinositide species such as phosphatidylinositol 4,5-bisphosphate [PtdIns(4,5)P_2] and phosphatidylinositol 3,4,5-trisphosphate [PtdIns(3,4,5)P_3][10]. TIPE3 can function as a PtdIns(4,5)P_2 transfer protein, i.e. it can extract PtdIns(4,5)P_2 from the lipid bilayer, accommodate the acyl chains of this lipid in the cavity and shuttle it through the aqueous solutions. This action of TIPE3 promotes PtdIns(4,5)P_2 phosphorylation by PI(3)Ks[10]. However, it is not clear if all TIPE family members could function as PtdIns(4,5)P_2 transfer proteins. In addition to interacting with phosphoinositides, TIPE2 can also directly bind and inhibit Rac[18]. TIPE2 is expressed primarily by bone marrow-derived cells and suppresses Toll-like receptor signaling through the interaction with Rac[18,19]. As a consequence, TIPE2-deficient cells are hyper-responsive to Toll-like receptor activation and have enhanced phagocytic and bactericidal activities, and TIPE2-deficient mice are hypersensitive to intravenously induced septic shock and resistant to intravenous bacterial infections[18,19].

Results

Defective chemotaxis of TIPE2 knockout leukocytes

To understand the role of TIPE2 in chemotaxis, we studied the migration of circulating *Tipe2*$^{-/-}$ and wild-type leukocytes into peritoneal cavity in a murine model of acute peritonitis. Significantly fewer TIPE2-deficient Ly6G^{+} myeloid cells migrated into the peritoneal cavity, leaving markedly more of them in the blood as compared to WT myeloid cells in the same mice (Fig. 1a). To study TIPE2-dependent chemotaxis *in vitro*, we used transwell chambers (for transmigration) and μ-slides (for two-dimensional chemotaxis). Murine *Tipe2*$^{-/-}$ bone marrow-derived macrophages (BMDMs) and bone marrow neutrophils (BMNs), and human TIPE2-deficient HL-60 neutrophils (dHL-60T) all showed significant defects in migration through transwell filters following chemoattractant

gradients, but did not exhibit any defect in random migration as compared to WT controls (Fig. 1b - d and Supplementary Fig. 1a). The chemotaxis defect of dHL-60T cells could be fully rescued by expressing a wild-type *TIPE2* transgene (Fig. 1d and Supplementary Fig. 1a). Importantly, in the μ-slide chemotaxis assay, *Tipe2*$^{-/-}$ neutrophils showed significant reductions in both directionality (by ~62% as compared to WT cells) and velocity (by ~25%) (Fig. 1e,f and Supplementary Fig. 1b,c). Taking together, these results indicate that TIPE2 controls leukocyte chemotaxis *in vivo* and *in vitro*.

Loss of polarization in TIPE2 knockout leukocytes

To explore how TIPE2 controls chemotaxis, we studied polarization of neutrophils in response to point-source chemoattractants. To visualize polarization, we expressed in cells an enhanced green fluorescent protein (eGFP)-tagged PtdIns(3,4,5)P_3-specific probe (the GRP1-PH domain), or stained cells for F-actin, Rac-GTP (the active form of Rac), or p-AKT(T308), the active form of AKT phosphorylated at threonine 308 that serves as an indicator of PI(3)K activation[2,3]. By time-lapse microscopy, we compared polarization of WT and TIPE2-deficient dHL-60 neutrophils in response to point-source CXCL8 stimulation over a period of 400 seconds (Fig. 2a and Supplementary Fig. 1d). CXCL8-induced polarization of WT dHL-60 control (dHL-60C) cells occurred almost immediately after chemokine exposure, with more than 60% of cells polarized 180 seconds later. Chemokine-induced polarization was markedly reduced in dHL-60T neutrophils, with only <14% of cells polarized at the end of the observation period.

Similarly, 150 seconds after the exposure to chemoattractants, the vast majority of wild-type BMNs were polarized, with F-actin, Rac-GTP, and p-AKT(T308) primarily localized at the leading edge of cells; by contrast, most *Tipe2*$^{-/-}$ BMNs were not polarized (Fig. 2b - g and Supplementary Fig. 2a - e). Importantly, the polarization defect of dHL-60T neutrophils could be rescued by expressing a wild-type *TIPE2* transgene (Supplementary Fig. 2f - h). TIPE2-deficient cells were sensitive to chemoattractant stimulation, as evidenced by elevated global abundance of p-AKT(T308) and F-actin (Fig. 2b,d,f, Supplementary Notes and Supplementary Figs. 2-4). In addition, in response to chemoattractant stimulation, *Tipe2*$^{-/-}$ BMNs increased their spreading areas more significantly, but failed to acquire an elongated shape as compared to wild-type BMNs (Fig. 3a). Taken together, these results indicate that TIPE2 controls the stable polarization of the signaling and actin regulatory molecules that are essential for the formation of the leading and trailing edges in chemotaxing neutrophils.

TIPE2 and Rac in leukocyte polarization

Inhibitory proteins of the chemoattractant-induced signaling and cytoskeletal activities are predicted to be essential for cell polarization and chemotaxis[1,4–6]. Consistent with our previous report, TIPE2 interacted with Rac in several cell types (Fig. 3b - d, and Supplementary Notes)[18]. We hypothesized that TIPE2-dependent inhibition of Rac was required for effective cell polarization[20]. Pretreatment of *Tipe2*$^{-/-}$ BMNs with a specific Rac inhibitor NSC24766 prior to chemokine stimulation significantly reduced cell spreading and abolished the difference in spreading areas between wild-type and *Tipe2*$^{-/-}$ BMNs (Fig. 3a). By contrast, PI(3)K inhibitor LY294002 did not have the same effect on cell spreading,

suggesting that TIPE2 controls cell spreading through the interaction with Rac (Fig. 3a). Importantly, Rac inhibition partially rescued the polarization defect of *Tipe2*$^{-/-}$ BMNs and dHL-60T. F-actin and p-AKT(T308) were excluded from the edges of the cells opposite to the source of chemoattractants (Fig. 3e - h and Supplementary Fig. 5a,b). Thus, TIPE2 served as a cellular Rac inhibitor, promoting trailing edge formation and suppressing the generation of secondary leading edges. However, *Tipe2*$^{-/-}$ BMNs and dHL-60T neutrophils treated with Rac inhibitor failed to form well-defined leading edges, strongly suggesting a Rac-GTP-independent role of TIPE2 in leading edge formation (Fig. 3e,f and Supplementary Fig. 5b). Importantly, TIPE2 exhibited a polarized localization in migrating BMNs, dHL-60C and TIPE2-expressing dHL-60T. It is highly enriched at the leading edge, although also present throughout the cells (Fig. 4a, and Supplementary Fig. 5c). Since the interaction of TIPE2 with Rac took place in both the cytoplasm and plasma membrane, we asked if Rac-GTP, localized exclusively at the leading edge, was responsible for the polarized localization of TIPE2. Rac inhibition did not significantly change the localization of TIPE2 (Fig. 4a,b and Supplementary Fig. 5b,c). However, pretreatment of wild-type BMNs, dHL-60C and TIPE2-expressing dHL-60T with a PI(3)K inhibitor abolished the polarized distribution of TIPE2 and F-actin (Fig. 4a,c-f and Supplementary Fig. 5c,d). By contrast, the PI(3)K inhibitor only slightly altered Rac-GTP distribution. Rac-GTP was enriched in the leading edge, but was also detected at the trailing edge at low amounts (Fig. 4a,c,e). These data suggest that Rac-independent, but PI(3)K-dependent mechanisms are likely responsible for the polarized TIPE2 localization in migrating cells. Taken together, our results indicate that TIPE2 may play dual roles in the polarization of migrating cells. TIPE2 controls the trailing edge formation through inhibition of Rac, and employs its Rac-independent, PI(3)K-dependent activities for the formation of the leading edge.

TIPE2-mediated PtdIns(4,5)P_2 transfer

To explore the Rac-independent actions of TIPE2 at leading edges, we investigated the functional significance of TIPE2 binding to phosphoinositides. We hypothesized that TIPE2 acted differently at membranes containing PtdIns(4,5)P_2 and PtdIns(4,5)P_2 plus PtdIns(3,4,5)P_3, which are characteristics of trailing and leading edges, respectively. Using small unilamellar vesicles (SUV) made of phospholipid bilayers, we found that TIPE2 protein could effectively bind to SUV containing 10% PtdIns(4,5)P_2 (with ~65% TIPE2 bound to the vesicle) and to a lesser extent to SUV containing 10% PtdIns(3,4,5)P_3 (with ~14% TIPE2 bound), but it only very weakly bound to SUV containing both 10% PtdIns(4,5)P_2 and 10% PtdIns(3,4,5)P_3 (with ~4% TIPE2 bound) (Fig. 5a and Supplementary Fig. 6a). Consistent with this finding, TIPE2 showed reduced binding to SUV containing 5% PtdIns(4,5)P_2 and 5% PtdIns(3,4,5)P_3 as compared to SUV containing 10% PtdIns(4,5)P_2 (Fig. 5a). TIPE2 did not bind SUV containing PtdIns(4)P or only phosphatidylcholine (PC) (Fig. 5a). Therefore, TIPE2 exhibited differential binding to SUV containing PtdIns(4,5)P_2, PtdIns(3,4,5)P_3, or both of the phosphoinositides. Previously, we demonstrated that positively charged residues of α0 helix of TIPE3 mediates the formation of electrostatic interactions with the negatively charged phosphate groups of phosphoinositides[10]. To evaluate whether positively charged residues of α0 helix of TIPE2 contributed to this protein's interaction with phosphoinositides, we generated TIPE2 K15/16Q mutant (15/16Q), in which lysines 15 and 16 in the α0 helix were replaced with

glutamines (Supplementary Fig. 6b). Similar to TIPE2, 15/16Q could strongly bind SUV containing 10% PtdIns(4,5)P_2 (Fig. 5a and Supplementary Fig. 6a). However, this mutant almost completely lost the binding to SUV containing 10% PtdIns(3,4,5)P_3 (Fig. 5a). In addition, 15/16Q could interact with PtdIns(4)P-containing SUV (Fig. 5a). To determine to what degree the α0 helix contributed to TIPE2 binding to phosphoinositides, we fused eGFP with wild-type or lysine-mutated TIPE2 α0 helix. We found that the TIPE2 α0 helix could interact with phosphoinositide-containing SUV with the following order of preference: PtdIns(3,4,5)P_3 > PtdIns(4,5)P_2 > PtdIns(4)P, and that lysine mutations within the α0 helix negated this interaction (Fig. 5b and Supplementary Fig. 6a). Importantly, unlike PtdIns(4,5)P_2 that showed markedly reduced binding to the α0 helix as compared to its binding to the full-length TIPE2, PtdIns(3,4,5)P_3 binding to the helix was similar to its binding to the full-length TIPE2 (Supplementary Fig. 6c). These results strongly suggest that TIPE2 interacts with PtdIns(3,4,5)P_3, but not PtdIns(4,5)P_2, mostly through the electrostatic interactions formed between positively charged amino acids of its α0 helix and negatively charged phosphate groups of the phosphoinositide.

We asked whether the marked reduction in TIPE2 binding to SUV containing both PtdIns(4,5)P_2 and PtdIns(3,4,5)P_3 resulted from PtdIns(3,4,5)P_3-dependant extraction of PtdIns(4,5)P_2 by TIPE2 from the vesicles. We hypothesized that the α0 helix of TIPE2 functioned as a flexible lid of its hydrophobic cavity, and that the conformational change induced by PtdIns(3,4,5)P_3 binding displaced the lid and allowed TIPE2 to extract PtdIns(4,5)P_2 from the lipid bilayer and transfer it to the solution[10,21]. Indeed, TIPE2 extracted and transferred PtdIns(4,5)P_2 from the SUV containing both PtdIns(4,5)P_2 and PtdIns(3,4,5)P_3, but not from SUV containing no PtdIns(3,4,5)P_3 (Fig. 5c). As expected, more than 81% of TIPE2 was not bound by SUV containing both PtdIns(4,5)P_2 and PtdIns(3,4,5)P_3, which was significantly reduced in the absence of PtdIns(3,4,5)P_3 in the SUV (Fig. 5d). Thus, TIPE2 may function as a PtdIns(4,5)P_2 transfer protein only on membranes that contain PtdIns(3,4,5)P_3, a characteristic of the leading edge of chemotaxing cells (Supplementary 6d).

TIPE2 in PtdIns(4,5)P_2 signaling and actin remodeling

Since TIPE2 is capable of both binding and extracting PtdIns(4,5)P_2, we examined whether TIPE2 could regulate PtdIns(4,5)P_2-dependent signaling. First, we analyzed the ability of TIPE2 to promote the phosphorylation of PtdIns(4,5)P_2 by active PI(3)Ks, a key process occurring at the leading edge of migrating cells. We found that TIPE2 indeed increased PI(3)K-catalyzed conversion of PtdIns(4,5)P_2 to PtdIns(3,4,5)P_3 for up to 5 fold, in a dose-dependent manner (Fig. 6a). 15/16Q that strongly bound PtdIns(4,5)P_2 but almost completely lost its ability to bind PtdIns(3,4,5)P_3 had a weak or no effect on PI(3)K-catalyzed PtdIns(3,4,5)P_3 generation (Fig. 6a). Second, we tested if, through its interaction with PtdIns(4,5)P_2 and PtdIns(3,4,5)P_3, TIPE2 could affect actin remodeling, which is required for leading edge formation. For this study we selected cofilin, an actin-severing protein, whose activity to drive actin remodeling is inhibited by its binding to phosphoinositides[22,23]. We found that TIPE2 binding to SUV containing either PtdIns(4,5)P_2 or PtdIns(3,4,5)P_3 led to a small decrease in the phosphoinositide interaction with cofilin (Fig. 6b,c). By contrast, the interaction of cofilin with SUV containing both

PtdIns(4,5)P_2 and PtdIns(3,4,5)P_3 was reduced for more than 7 fold by TIPE2 (Fig. 6b,c). The effect of 15/16Q on the cofilin binding to the vesicles was similar to that of wild-type TIPE2, but to a lesser degree, due presumably to its weakened binding to phosphoinositides (Fig. 6b,c). The expression of 15/16Q in dHL-60T neutrophils only partially rescued the polarization defect (Supplementary Fig. 6e).

To understand the impact of TIPE2 binding to phosphoinositides on cofilin activity, we examined cofilin-induced F-actin depolymerization in the presence or absence of purified TIPE2 protein and phosphoinositides. SUV containing either PtdIns(4,5)P_2 or PtdIns(4,5)P_2 plus PtdIns(3,4,5)P_3 significantly decreased cofilin-induced F-actin depolymerization (Fig. 6d,e and Supplementary Fig. 7a,b). However, TIPE2 could only rescue the decrease in F-actin depolymerization caused by SUV containing both PtdIns(4,5)P_2 and PtdIns(3,4,5)P_3 (Fig. 6d,e and Supplementary Fig. 7a,b). PtdIns(3,4,5)P_3, TIPE2, or control protein alone had no effect on F-actin depolymerization (Fig. 6f, Supplementary Fig. 7c, and data not shown). These results indicate that the ability of TIPE2 to extract PtdIns(4,5)P_2 from PtdIns(3,4,5)P_3-rich membranes impacts cofilin-induced F-actin remodeling.

TIPE2 in neural inflammation

Directional migration of leukocytes into the central nervous system is crucial for the development of multiple sclerosis in humans, and experimental autoimmune encephalomyelitis (EAE) in mice[24,25]. Importantly, *Tipe2*$^{-/-}$ mice exhibited significantly delayed EAE onset and reduced clinical score relative to wild-type mice (Fig. 7a). Histological examination of spinal cord sections of mice with EAE revealed more severe leukocyte infiltration in the wild-type group than in the *Tipe2*$^{-/-}$ group (Fig. 7b). Bone marrow chimeric experiments established that TIPE2 expressed by bone marrow-derived cells contributed to the difference in EAE between wild-type and *Tipe2*$^{-/-}$ mice. Wild-type mice that received *Tipe2*$^{-/-}$ bone marrow cells developed significantly delayed and diminished EAE as compared to wild-type mice that received wild-type bone marrow cells (Fig. 7c). Importantly, the resistance of *Tipe2*$^{-/-}$ mice to EAE was not caused by a reduction in T cell responses to myelin oligodendrocyte glycoprotein (MOG). *Tipe2*$^{-/-}$ splenocytes isolated from mice 9 days after the EAE induction produced normal or slightly increased concentrations of interleukin 2 (IL-2), interferon-γ and IL-17 after MOG-stimulation *in vitro*, as compared to wild-type splenocytes (Supplementary Fig. 8). To test whether reduced EAE in *Tipe2*$^{-/-}$ mice could be related to decreased leukocyte migration, we generated mixed bone marrow chimeric mice containing both *Tipe2*$^{-/-}$ and wild-type bone marrow-derived cells. At EAE onset, we observed significantly less *Tipe2*$^{-/-}$ total and CD11b^{+}Ly6G^{+} leukocytes present in the spinal cord as compared to wild-type cells in the same mice (Fig. 7d,e). Thus, TIPE2 plays a crucial role in controlling leukocyte infiltration during neural inflammation.

Discussion

Leukocyte chemotaxis is essential for immune defense and surveillance[26–28]. Effective pathogen elimination and tissue repair depend on well-coordinated leukocyte chemotaxis, and its dysregulation can lead to severe infectious diseases. On the other hand, directed

leukocyte migration into inflamed tissues is a common pathological process of many autoimmune diseases. Blocking leukocyte chemotaxis using the drug natalizumab or fingolimod is effective for treating autoimmune diseases such as multiple sclerosis. Therefore, understanding the molecular events regulating chemotaxis can help identify new drug targets for treating inflammatory and infectious disorders[26,28].

Several lines of evidence presented in this study establish that TIPE2, a phosphoinositide transfer protein of TIPE family, controls leukocyte chemotaxis by acting as a polarizer, or a dual-role regulator of signaling and cytoskeletal activities, in chemotaxing cells. TIPE2 acts as a Rac inhibitor, suppressing Rac-dependent actin polymerization and PI(3)Kp110β–AKT activation[29–31]. This action of TIPE2 promotes the formation of trailing edges, and prevents the generation of secondary leading edges. TIPE2 can also function as a PtdIns(4,5)P_2 transfer protein, extracting PtdIns(4,5)P_2 from PtdIns(3,4,5)P_3-containing membranes and shuttling it in its hydrophobic cavity. This latter activity of TIPE2 is likely "excited" by PtdIns(3,4,5)P_3 generated locally by PI(3)Kp110γ, a kinase responsible for the early phase PtdIns(3,4,5)P_3 generation in response to GPCR activation[31–33]. By "presenting" PtdIns(4,5)P_2 to PI(3)Ks and enhancing the generation of PtdIns(3,4,5)P_3 at PtdIns(3,4,5)P_3-containing membranes, TIPE2 reinforces a positive feedback loop that amplifies the PI(3)K signaling. PtdIns(3,4,5)P_3 in turn activates Rac guanine-nucleotide-exchange factors (RacGEFs), resulting in Rac activation and subsequent actin polymerization at the PtdIns(3,4,5)P_3-rich leading edges[2]. Additionally, TIPE2 also enhances actin dynamics by extracting PtdIns(4,5)P_2 from PtdIns(3,4,5)P_3-rich membranes, sequestering it from actin-modifying proteins, thereby further promoting leading edge formation. Recent work indicates that decreasing PtdIns(4,5)P_2 abundance lowers the threshold for excitability of the signaling network and promotes the formation of leading edge protrusions[34]. It is possible that by extracting PtdIns(4,5)P_2 from PtdIns(3,4,5)P_3-rich membranes alone, TIPE2 contributes to leading edge formation. Therefore, using a coincidence-detection strategy (i.e., active only when both PtdIns(4,5)P_2 and PtdIns(3,4,5)P_3 are present) TIPE2 enhances the GPCR signaling only at the side of the cell facing the source of chemoattractants and guides the leading edge formation in a spatial-specific manner. These findings are consistent with the proposed models of chemotaxis on flat two-dimensional surfaces that predict the existence of both local enhancers and global inhibitors that are required for directional migration[1,4–6].

Tipe2$^{-/-}$ myeloid cells exhibited impaired chemotaxis in comparison with wild-type cells in two *in vivo* models, namely the acute peritonitis model and EAE. Leukocytes migrate through different tissues characterized by diverse composition and geometry to reach sites of inflammation. To acquire mechanistic information of chemotaxis, we utilized *in vitro* two-dimensional systems. However, these systems may not fully reflect the diversity and complexity of tissues *in vivo*[35–37]. For example, PI(3)K is much more critical for chemotaxis *in vivo* than in two-dimensional systems[38]. At the same time, branched F-actin that is essential for chemotaxis on two-dimensional surfaces plays a role only in directional selection in three-dimensional systems[35–37]. Future studies of the TIPE2-dependent effects in other models of leukocyte migration may help further elucidate the mechanisms of chemotaxis regulation *in vivo*.

Results reported here indicate that TIPE2 plays a crucial role in leukocyte infiltration of neural tissue in EAE. Although this is likely mediated through chemotaxis, TIPE2 may also regulate EAE through additional mechanisms. For example, MOG-specific T cell responses in TIPE2-deficient mice were slightly enhanced as compared to wild-type mice. This result is consistent with previous reports that TIPE2 is important for preventing immune hyper-responsiveness[18,19,39]. TIPE2 regulation of Rac is likely involved in both chemotaxis and control of hyper-responsiveness during EAE. Taken together, TIPE2 is crucial for organ-specific inflammation, and TIPE2 inhibition may be beneficial for the treatment of inflammatory diseases such as multiple sclerosis.

Methods

Mice

Tipe2$^{-/-}$ C57BL/6 mice were generated as described[18,19]. Wild-type C57BL/6 mice expressing CD45.1 or CD45.2 were purchased from Jackson Laboratories. Mice were housed in the University of Pennsylvania Animal Care Facilities under pathogen-free conditions. All animal procedures were preapproved by the Institutional Animal Care and Use Committee of the University of Pennsylvania, and all experiments conform to the relevant regulatory standards.

The acute peritonitis model for studying myeloid cell migration *in vivo*

Six-week-old wild-type CD45.1^{+} mice (recipient mice) were injected intraperitoneally with Freund's adjuvant (0.5 ml/mouse) to induce acute peritonitis. Twenty-four hours later, they were injected intravenously with carboxyfluorescein succinimidyl ester (CFSE)-labeled bone marrow cells (10^7/mouse) from 6-week-old *Tipe2*$^{-/-}$ CD45.2^{+} and wild-type CD45.1^{+} mice, mixed at 1:1 ratio. Recipient mice were sacrificed 16 h later, and their peritoneal cells were collected. The peritoneal cells were stained with anti-CD45.1-PE (eBioscience), anti-CD45.2-PerCP/Cy5.5 (eBioscience), and anti-Ly6G-APC (eBioscience), and the percentages of *Tipe2*$^{-/-}$CD45.2^{+}CFSE^{+}Ly6G^{+} and wild-type CD45.1^{+}CFSE^{+}Ly6G^{+} cells were determined by flow cytometry. The number of mice required for the experiment was calculated using the Power and Sample Size Calculation (PS) software (Vanderbilt University). The paired Student *t*-test was used to assess the statistical significance of the results.

Experimental autoimmune encephalomyelitis (EAE)

The induction and clinical scoring of EAE in wild-type and *Tipe2*$^{-/-}$ mice were performed as we described previously[40,41]. Myelin oligodendrocyte glycoprotein (MOG) 35–55 peptide was used as the autoantigen. Spinal cords of mice were harvested at the end of each experiment, fixed, paraffin-embedded, and sectioned. The sections were stained with hematoxylin and eosin, and analyzed using a wide field light microscope. To determine the contribution of TIPE2 expressed by bone marrow-derived cells in EAE, a bone marrow chimeric approach as we described was used[42]. Briefly, wild-type mice were sub-lethally irradiated and injected intravenously with bone marrow cells from *Tipe2*$^{-/-}$ or wild-type mice (1.5×10^7 cells/mouse). Seven weeks later, EAE was induced and examined as

described[40,41]. The number of mice used for the experiments was calculated using the PS software. Mann-Whitley *U* test was used to assess the statistical significance of the results.

To study wild-type and *Tipe2*$^{-/-}$ leukocyte migration in mice with EAE, a mixed bone marrow chimeric approach as we described was used[42]. Briefly, 6-week-old wild-type CD45.1^{+} mice (recipient mice) were sub-lethally irradiated and injected intravenously with bone marrow cells of 6-week-old *Tipe2*$^{-/-}$ CD45.2^{+} and wild-type CD45.1^{+} mice, mixed at 1:1 ratio (1.5×10^7 cells/mouse). Seven weeks later, the recipient mice were immunized with MOG to induce EAE, and sacrificed on the day of the disease onset (with a clinical EAE score of 1). Blood and spinal cords (collected after perfusion of recipient mice with 30 ml PBS via the heart) of recipient mice were used for leukocyte isolation by centrifugation through a Percoll gradient. The blood and peritoneal leukocytes were stained with anti-CD45.1-PE (eBioscience) and anti-CD45.2-PerCP/Cy5.5 (eBioscience) or with anti-CD45.1-PE (eBioscience), anti-CD45.2-PerCP/Cy5.5 (eBioscience), anti-Ly6G-APC (eBioscience) and anti-CD11b-FITC (eBioscience) antibodies, and percentages of total *Tipe2*$^{-/-}$ CD45.2^{+} and wild-type *CD45.1*$^{+}$ leukocytes or *Tipe2*$^{-/-}$ CD45.2^{+}CFSE^{+}Ly6G^{+} and wild-type CD45.1^{+}CFSE^{+}Ly6G cells, respectively, among total leukocytes were determined by flow cytometry. Numbers of mice ($n = 3$) required for the experiments were estimated using the PS software (Vanderbilt University). Student's *t*-test was used to assess the statistical significance of the results.

Generation of bone marrow-derived macrophages (BMDMs), plasmid DNA transfection, retrovirus preparation and infection, immunoblotting, co-immunoprecipitation, and ELISA

Assays were performed as we previously described[10,18,43]. The purity of BMDMs populations was greater than 95% as determined by flow cytometry after staining cells with anti-CD11b-FITC (eBioscience) and anti-F4/80-APC (eBioscience), and the viability was greater than 99% as determined by trypan blue staining. Antibodies to the following antigens were used for immunoblotting and co-immunoprecipitation: Rac1 (EMD Millipore), Rac1/2/3, RhoGDI, AKT, p-AKT (T308), p-AKT (S473), p-GSK-3β (S9), cofilin, p-cofilin (S3), p-PAK1/2 (S144/S141), p-LIMK1 (Thr508)/LIMK2 (Thr505), ERK1/2, p-ERK1/2 (T202/Y204), p-p38 (T180/Y182), mTOR, GAPDH, integrin-β1 (Cell Signaling Technology), TIPE2 (Proteintech), Flag, actin (Sigma-Aldrich,), HA (Cell Signaling Technology). Control IgG (Santa Cruz Biotechnology) anti-rabbit IgG-HRP, and anti-mouse IgG-HRP (GE Healthcare Life Sciences) were also used.

Isolation of bone marrow neutrophils (BMNs) and blood neutrophils (BNs)

Murine blood was drawn from retro-orbital plexus of the eyes, and bone marrow was collected from femur and tibia bones. BNs and BMNs were isolated using Histopaque-1119 and Histopaque-1077 (Sigma-Aldrich) according to the manufacturer's instructions. The purity of BNs and BMNs populations was greater than 90% as determined by flow cytometry after staining with anti-Ly6G-APC (eBioscience), and the viability was greater than 99% as determined by trypan blue staining.

Generation of TIPE2-deficient HL-60 (HL-60T), TIPE2-expressing and 15/16Q-expressing HL-60T cells

HL-60 cells were obtained from ATCC and cultured in RPMI-1640 supplemented with 15% fetal bovine serum. TIPE2-deficient HL-60 cells (HL-60T) and control HL-60 cells (HL-60C) were generated using CRISPR/Cas9 system and TIPE2-specific single guide RNA (sgTIPE2) or non-targeting control single guide RNA (sgControl) as described[44]. To generate TIPE2-expressing or 15/16Q-expressing HL-60T (TIPE2-HL-60T) cells, HL-60T cells were infected with retroviruses that carried either TIPE2 or 15/16Q and nerve growth factor receptor (NGFR) cDNAs. Control HL-60C cells were infected with retroviruses that carried NGFR cDNA alone (a gift from W. Pear, University of Pennsylvania). $NGFR^+$ cells were isolated by FACS. Before being used in the assays, HL-60 cells were treated with 1.25% DMSO and 25 ng/ml G-CSF for 5 days to generate differentiated HL-60 neutrophils (dHL-60)[45].

Transwell migration assay

For BMDMs, cells were rested in DMEM for 1 h. For BMNs, cells were rested in Hanks' Balanced Salt solution (HBSS) containing 0.1% BSA (fatty acid free) for 1 h. For dHL-60C, dHL-60T, and TIPE2-expressing dHL-60T, cells were stained with Calcein-AM (BD Biosciences) and rested in HBSS containing 0.1% BSA for 30 min. After resting, migration assays were performed using transwells with 5.0 μm-pore filters (for BMDMs and BMNs) or 3.0 μm-pore filters (for dHL-60), which were coated with fibronectin (Corning)[46]. For BMDMs, CCL2 was added to the bottom wells at the concentration of 10, 20 or 40 ng/ml. For BMNs, CXCL2 was added at the concentration of 10 or 50 ng/ml. For dHL-60, CXCL8 was added at the concentration of 25 ng/ml. Cells were allowed to migrate for 0.5–3 h, and those migrated into the lower chamber were counted. Chemotaxis index = the number of cells that migrated in response to chemoattractant / the number of cells that migrated randomly (in the absence of chemoattractants). Student's *t*-test was used to assess the statistical significance of the results.

μ-slides migration assays

Wild-type and *Tipe2*$^{-/-}$ BN were resuspended in RPMI medium supplemented with 2% FBS, rested for 30 min and then loaded into μ–slides (Ibidi) following the manufacturer's instructions. CXCL1 was added only into one reservoir of the μ–slide at the concentration of 200 ng/ml. Cells were recorded every 45 sec for at least 2 h using a Leica DMI4000 microscope with Yokogawa CSU-X1 spinning disk confocal attachment at 10× magnification. Images were analyzed by Volocity software (Perkin Elmer) using the automated tracking protocol. Objects less than 16 μm^3 were excluded, and tracks were generated with the shortest path model. A maximum distance between objects was set to 25 μm, based on observed optimal tracking in the wild-type cells. Tracks less than 200 μm were excluded. Cell velocity and vector angle between each track's starting and end points were obtained from Volocity using these settings. Velocity was defined as a cell's centroid movement in μm/min along the total path. Cell directionality, or directional movement index (DMI), was defined as the cosine of the vector angle formed by the line between the cell's start point and the source of the chemoattractant, and the line between the cell's start point

and the end point. A value of 1 indicates migration directly towards the chemoattractant, while a value of −1 indicates migration away from the chemoattractant. To generate representative center-zeroed tracks of individual wild-type and *Tipe2*$^{-/-}$ cells, a subset of all the tracks used in the analysis was displayed to avoid oversaturation of the image. The tracks were sorted by migration length and the tracks with 40 longest migration lengths were displayed for each genetic background. Tracks with lengths greater than 400 μm in length were excluded, and tracks were only selected from the middle of the videos (track time 25–80 min). None of these exclusions were made for the quantitative analyses. The results of a representative experiment are shown. The statistical significance of the results was evaluated by Mann-Whitney *U* test (directionality) and Student's *t*-test (velocity).

Time-lapse confocal microscopy of live neutrophils

The polarization of PtdIns(3,4,5)P_3 in migrating cells was visualized by eGFP-tagged GRP1-PH domain, which specifically binds PtdIns(3,4,5)P_3. Briefly, dHL-60C and dHL-60T neutrophils were transfected with peGFP-GRP1-PH vector (kindly provided by M. Lemmon, University of Pennsylvania) using Amaxa cell line nucleofector kit V (Lonza) and Amaxa nucleofector II (program Y-001, Lonza). Cells were plated onto fibronectin-coated glass bottom dishes 24 h after transfection. The adherent dHL-60C and dHL-60T cells were subjected to point-source stimulation with 125 ng/ml CXCL8 at 37 °C. The migration of dHL-60C and dHL-60T neutrophils along the CXCL8 gradient was recorded every 10 sec for at least 400 sec using an Olympus IX71 inverted fluorescent microscope with spinning disk confocal attachment at 60× magnification. The images were analyzed using ImageJ software. The experiment was repeated two times. More than 45 cells of each genotype were analyzed. Cell polarization was determined based on the line fluorescence intensity profile of cells. Cells were considered polarized if the average fluorescence signal on one side of the cell was more than 1.5 times stronger than the signal on the opposite side. Results are presented as the degree of CXCL8-induced PtdIns(3,4,5)P_3 polarization, which is the difference in the percentage of polarized cells before and after stimulation with CXCL8. The statistical significance of results was evaluated by Mann-Whitney *U* test.

Immunofluorescence analysis and confocal microscopy of fixed neutrophils

BMNs, dHL-60C, dHL-60T, TIPE2-expressing and 15/16Q-expressing dHL-60T cells were rested for 1 h in HBSS containing 0.1% BSA. Then cells were subjected to point-source stimulation with CXCL2 or CXCL8 at 1 μg/ml for 2.5 min at 37 °C[33]. In several experiments before stimulation with chemoattractants, BMNs and dHL-60 were pretreated with vehicle, Rac inhibitor (NSC24766, 200 μM, Tocris) or with PI(3)K inhibitor (LY29004, 25 μM, Cell Signaling Technology) for 30 min. After stimulation, cells were fixed with 3% paraformaldehyde in Phosphate-Buffered Saline (PBS) for 15 min at 37 °C, permeabilized in PBS containing 0.1 % Triton X-100 and 3% BSA for 10 min at 25 °C and blocked with PBS containing 5% normal goat serum and 3% BSA for 1 h at 25 °C. BMNs and dHL-60 cells were stained overnight at 4 °C with Phalloidin-AlexaFluor 555 (Cell Signaling Technology) in 3% BSA. Alternatively, they were first incubated overnight at 4 °C with anti-pAKT(T308) (Cell Signaling Techology), anti-TIPE2 (Proteintech), or anti-Rac-GTP (NewEast Biosciences) in 3% BSA, and then for 1 h at 25 °C with secondary anti-rabbit IgG Fab-AlexaFluor 555, anti-rabbit IgG Fab-AlexaFluor 555, or anti-mouse IgM Fab-Alexa Fluor

488 (ThermoFisher Scientific) in 3% BSA. Isotype-matched Igs, PI(3)K inhibitor-treated cells, and Rac inhibitor-treated cells were used as staining controls. Slides were dried and covered with ProLong Gold with DAPI (Invitrogen). Images were acquired on a Zeiss LSM 510 NLO/META and Zeiss LSM 710 confocal microscope and analyzed using LSM Image Browser, Zen lite (Zeiss), and ImageJ software. All images shown are representatives of at least two independent experiments. Thirty to 120 cells of each type and condition were analyzed. Cell polarization was evaluated as described above. Results are presented as the percentages of cells of each genotype with polarized or unpolarized distributions. The statistical significance of the results was evaluated by X^2 test. For F-actin polarization, results are also presented as the degree of chemoattractant-induced F-actin polarization, which is the difference in the percentage of polarized cells before and after stimulation with chemoattractant. Student's *t*-test was used to assess the statistical significance of these results. To study the spreading of wild-type and *Tipe2*$^{-/-}$ BMNs, more than thirty cells of each type and condition were measured. The spreading value of the resting wild-type BMNs was set to 1. The statistical significance of results was evaluated by Mann-Whitney *U* test.

Adhesion assay of BMDMs and dHL-60 cells

For wild-type and *Tipe2*$^{-/-}$ BMDMs, cells were cultured overnight in DMEM medium supplemented with 10% fetal bovine serum, collected with 5 mM EDTA in DPBS, and rested in DMEM for 1 h. Adhesion to fibronectin-coated plates of rested or rested and stimulated cells (with 20 ng/ml of CCL2) was assessed by staining adherent cells with crystal violet and measuring absorbance at 570 nm. The adhesion value of wild-type BMDMs at 15 min was set to 1. For dHL-60C, dHL-60T and TIPE2-expressing dHL-60T, cells were labeled with 0.5 μM calcein-acetoxymethyl ester (Molecular Probes) for 30 min at 37 °C and pretreated with vehicle, Rac inhibitor or with PI(3)K inhibitor for 2 h at 37 °C. Then, cells were added to plates coated with fibronectin and incubated for 5 min at 37 °C. Relative numbers of dHL-60, dHL-60T and TIPE2-expressing dHL-60T adherent to fibronectin were determined in a fluorescence multi-well plate reader (Molecular Devices). The adhesion value of dHL-60C pretreated with vehicle was set to 1. Student's *t*-test was used to assess the statistical significance of the results at each time point.

Flow cytometric analysis of F-actin and pAKT(308) cellular content

Wild-type and *Tipe2*$^{-/-}$ murine BMNs or dHL-60T and TIPE2-expressing dHL-60T cells were rested in HBSS containing 0.1% BSA. Cells were treated with or without fMLP (10 μM) or CXCL2 (100 ng/ml) for 30, 60, 120 and 300 sec. Cells were then fixed in PBS containing 4% paraformaldehyde overnight at 4 C° and permeabilized in PBS containing 0.1% Triton X-100 for 5 min at 25 °C. Cells were stained with rabbit anti-pAKT(T308) (Cell Signaling Technology) or control IgG (Santa Cruz biotechnology) for 1 h at 25 °C, and with anti-rabbit antibody labeled with AlexaFluor 488, Phalloidin-AlexaFluor 555, and anti-Ly6G-APC for 1 h at 25 °C, and analyzed by flow cytometry. Student's *t*-test was used to assess the statistical significance of the results at each time point.

Phosphoinositide binding and extraction assays

Recombinant His_6-TIPE2 15/16Q protein was generated by replacing lysines 15 and 16 with glutamines in wild-type His_6-TIPE2 protein. Recombinant His_6-α0-eGFP, His_6-α0 15/16Q-

eGFP and His_6-α0 4Q-eGFP proteins were generated by fusing enhanced green fluorescent protein (eGFP) with wild-type TIPE2 α0 helix or mutated TIPE2 α0 helix, in which lysines 15 and 16 (15/16Q), or lysines 15,16, 20 plus arginine 24 (4Q) were replaced with glutamines. His_6-TIPE2 (TIPE2), His_6-TIPE2 15/16Q (15/16Q), His_6-α0-eGFP (α0-eGFP), His_6-α0 15/16Q-eGFP (α0 15/16Q-eGFP), His_6-α0 4Q-eGFP (α0 4Q-eGFP) and His_6-cofilin (cofilin) were expressed in *Escherichia coli* BL21(DE3) cells (Stratagene), purified using Ni-charged MagBeads (GenScript), and dialyzed using Amicon Centrifugal Filters. Purified trypsin inhibitor of *Glycine max* was used as a control protein (Sigma-Aldrich). The small unilamellar vesicles (SUV) were produced and sedimentation-based phosphoinositide binding and extraction assays were performed as we previously described[10]. In sedimentation-based phosphoinositide binding assay, TIPE2, 15/16Q, control protein (trypsin inhibitor), α0-eGFP, α0 15/16Q-eGFP and α0 4Q-eGFP were used at concentration of 10 μM, and SUV were used at the concentration of 1 mM (0.5 mM total available lipid). In sedimentation-based phosphoinositide binding assay of cofilin, 1 mM SUV (0.5 mM total available lipid) were pretreated with 5 μM TIPE2, 15/16Q, control protein, or buffer alone for 1 h; then 5 μM cofilin was added to each reaction. After 20 min of incubation, samples were subjected to ultracentrifugation[47]. In sedimentation-based PtdIns(4,5)P_2 extraction assays, TIPE2 and control protein were used at the concentration of 10 μM and SUV containing fluorescently-labeled PtdIns(4,5)P_2 (TopFluor (TF)-PtdIns(4,5)P_2) were used at the concentration of 0.2 mM vesicles (0.1 mM total available lipid). Student's *t*-test was used to assess the statistical significance of the results.

PI(3)K enzymatic assay

PI(3)K enzymatic assays were performed as we previously described[10,48] with minor modifications: i.e., PI(3)K was assayed at a concentration of 4 μg/ml and SUV were used at a concentration of 125 μM. PI(3)K-catalyzed generation of PtdIns(3,4,5)P_3 determined at 40 min in the absence of TIPE2 or 15/16Q was set to 1. Student's *t*-test was used to assess the statistical significance of the results.

F-actin depolymerization assay

Actin Polymerization Biochem kit (Cytoskeleton) was used to investigate F-actin depolymerization by cofilin in the absence or presence TIPE2, control protein BSA and SUV containing 10% PtdIns(4,5)P_2, 10% PtdIns(3,4,5)P_3 or 10% PtdIns(4,5)P_2/10% PtdIns(3,4,5)P_3, according to the manufacturer's instructions with minor modifications. 2 mM SUV (1 mM total available lipid) were pretreated with 11 μM TIPE2 protein or control protein for 1 h; then cofilin (11 μM) was added to each reaction and incubated for 20 min. Additionally, cofilin (11 μM) was also incubated with TIPE2 (11 μM) or control protein (11 μM) for 20 min (control reactions). Pyrene-labeled F-actin stock was diluted with General Actin Buffer (25 mM Tris-HCl pH 8.0, 0.2 mM $CaCl_2$) to the concentration of 0.1 mg/ml. For each sample, 100 μl of diluted pyrene-labeled F-actin stock was used. The fluorescence was measured using an infinite 200 Pro fluorescence plate reader (Tecan) immediately before and after adding 10 μl of one of the following reagents: (a) control protein (22 μM), (b) cofilin (11 μM) + control protein (11 μM), (c) cofilin (11 μM) + TIPE2 (11 μM), (d) cofilin (11 μM) + control protein (11 μM) + SUV, (e) cofilin (11 μM) + TIPE2 (11 μM) + SUV, or (f) vehicle (25 mM HEPES, 150 mM NaCl, pH 7.5). The experiments were

performed in duplicates or triplicates and repeated at least four times. The results of a representative experiment are shown. The fluorescence measurements of each sample before adding the above reagents were set as 100%. The results were fitted to one-phase exponential decay equations using GraphPad Prism to assess the degree (or span) of F-actin depolymerization for each sample, which was calculated as differences in fluorescence before and after adding the above reagents. Student's *t*-test was used to assess the statistical significance of the results. Additionally, results are also presented as the differences in the remaining F-actin over a period of time. TIPE2, control protein, and SUV alone did not affect F-actin depolymerization, which is not shown.

Data availability—The data that support the findings of this study are available from the corresponding author upon request.

Supplementary Material

Refer to Web version on PubMed Central for supplementary material.

Acknowledgments

We thank M. Lemmon, G. Luo, N. Li, D. Johnson, A. Stout, J. Zhao, G. Ruthel, W. Pear, the CDB Microscopy Core, and the PennVet Imaging Core for discussions and/or technical assistance. This work was funded by the National Institutes of Health, USA (grants AI121166, AI099216, and AI50059) and National Multiple Sclerosis Society, USA (grant 1501-02782) to Y.H.C. A.E.B. was supported by T32CA009140.

References

1. Swaney KF, Huang C-H, Devreotes PN. Eukaryotic Chemotaxis: A Network of Signaling Pathways Controls Motility, Directional Sensing, and Polarity. Annu. Rev. Biophys. 2010; 39:265–289. [PubMed: 20192768]
2. Merlot S, Firtel RA. Leading the way: Directional sensing through phosphatidylinositol 3-kinase and other signaling pathways. J. Cell Sci. 2003; 116:3471–3478. [PubMed: 12893811]
3. Deng Q, Huttenlocher A. Leukocyte migration from a fish eye's view. J. Cell Sci. 2012; 125:3949–3956. [PubMed: 23104739]
4. Iglesias PA, Devreotes PN. Biased excitable networks: How cells direct motion in response to gradients. Curr. Opin. Cell Biol. 2012; 24:245–253. [PubMed: 22154943]
5. Huang C-H, Tang M, Shi C, Iglesias Pa, Devreotes PN. An excitable signal integrator couples to an idling cytoskeletal oscillator to drive cell migration. Nat. Cell Biol. 2013; 15:1307–1316. [PubMed: 24142103]
6. Tang M, et al. Evolutionarily conserved coupling of adaptive and excitable networks mediates eukaryotic chemotaxis. Nat. Commun. 2014; 5:5175. [PubMed: 25346418]
7. Ahn S-H, et al. Two Genes on A/J Chromosome 18 Are Associated with Susceptibility to Staphylococcus aureus Infection by Combined Microarray and QTL Analyses. PLoS Pathog. 2010; 6:e1001088. [PubMed: 20824097]
8. Zhang C, et al. Role of SCC-S2 in experimental metastasis and modulation of VEGFR-2, MMP-1, and MMP-9 expression. Mol. Ther. 2006; 13:947–955. [PubMed: 16455304]
9. Zhang Y, et al. Tumor Necrosis Factor-α Induced Protein 8 Polymorphism and Risk of Non-Hodgkin's Lymphoma in a Chinese Population: A Case-Control Study. PLoS One. 2012; 7:e37846. [PubMed: 22666399]
10. Fayngerts, Sa, et al. TIPE3 is the transfer protein of lipid second messengers that promote cancer. Cancer Cell. 2014; 26:465–478. [PubMed: 25242044]
11. Ma Y, et al. The Expression and Significance of TIPE2 in Peripheral Blood Mononuclear Cells from Asthmatic Children. Scand. J. Immunol. 2013; 78:523–528. [PubMed: 24107080]

12. Wang L, Song Y, Men X. Variance of TNFAIP8 expression between tumor tissues and tumor-infiltrating CD4+ and CD8+ T cells in non-small cell lung cancer. Tumour Biol. 2014; 35:2319–2325. [PubMed: 24136748]
13. Xi W, et al. Roles of TIPE2 in hepatitis B virus-induced hepatic inflammation in humans and mice. Mol. Immunol. 2011; 48:1203–1208. [PubMed: 21466895]
14. Yang M, et al. TNFAIP8 overexpression is associated with lymph node metastasis and poor prognosis in intestinal-type gastric adenocarcinoma. Histopathology. 2014; 65:517–526. [PubMed: 24621012]
15. Zhang C, et al. The significance of TNFAIP8 in prostate cancer response to radiation and docetaxel and disease recurrence. Int. J. Cancer. 2013; 133:31–42. [PubMed: 23280553]
16. Gus-Brautbar Y, et al. The anti-inflammatory TIPE2 is an inhibitor of the oncogenic Ras. Mol. Cell. 2012; 45:610–618. [PubMed: 22326055]
17. Zhang X, et al. Crystal structure of TIPE2 provides insights into immune homeostasis. Nat. Struct. Mol. Biol. 2009; 16:89–90. [PubMed: 19079267]
18. Wang Z, et al. TIPE2 protein serves as a negative regulator of phagocytosis and oxidative burst during infection. Proc. Natl. Acad. Sci. U. S. A. 2012; 109:15413–15418. [PubMed: 22949657]
19. Sun H, et al. TIPE2, a Negative Regulator of Innate and Adaptive Immunity that Maintains Immune Homeostasis. Cell. 2008; 133:415–426. [PubMed: 18455983]
20. Wrighton KH. Sensing and controlling protein dynamics. Nat. Rev. Mol. Cell Biol. 2010; 11:680–681.
21. Schaaf G, et al. Functional anatomy of phospholipid binding and regulation of phosphoinositide homeostasis by proteins of the sec14 superfamily. Mol. Cell. 2008; 29:191–206. [PubMed: 18243114]
22. Ghosh M, et al. Cofilin promotes actin polymerization and defines the direction of cell motility. Science. 2004; 304:743–746. [PubMed: 15118165]
23. Bravo-Cordero JJ, Magalhaes MAO, Eddy RJ, Hodgson L, Condeelis J. Functions of cofilin in cell locomotion and invasion. Nat. Rev. Mol. Cell Biol. 2013; 14:405–417. [PubMed: 23778968]
24. Steinbach K, Piedavent M, Bauer S, Neumann JT, Friese MA. Neutrophils Amplify Autoimmune Central Nervous System Infiltrates by Maturing Local APCs. J. Immunol. 2013; 191:4531–4539. [PubMed: 24062488]
25. Steinman L. Multiple sclerosis: a two-stage disease. Nat. Immunol. 2001; 2:762–764. [PubMed: 11526378]
26. Luster AD, Alon R, von Andrian UH. Immune cell migration in inflammation: present and future therapeutic targets. Nat. Immunol. 2005; 6:1182–1190. [PubMed: 16369557]
27. Friedl P, Weigelin B. Interstitial leukocyte migration and immune function. Nat. Immunol. 2008; 9:960–969. [PubMed: 18711433]
28. de Oliveira S, Rosowski EE, Huttenlocher A. Neutrophil migration in infection and wound repair: going forward in reverse. Nat. Rev. Immunol. 2016; 16:378–391. [PubMed: 27231052]
29. Fritsch R, et al. RAS and RHO families of GTPases directly regulate distinct phosphoinositide 3-kinase isoforms. Cell. 2013; 153:1050–1063. [PubMed: 23706742]
30. Sadhu C, Masinovsky B, Dick K, Sowell CG, Staunton DE. Essential role of phosphoinositide 3-kinase delta in neutrophil directional movement. J. Immunol. 2003; 170:2647–2654. [PubMed: 12594293]
31. Boulven I, et al. Class IA phosphatidylinositide 3-kinases, rather than p110 gamma, regulate formyl-methionyl-leucyl-phenylalanine-stimulated chemotaxis and superoxide production in differentiated neutrophil-like PLB-985 cells. J. Immunol. 2006; 176:7621–7627. [PubMed: 16751409]
32. Ferguson GJ, et al. PI(3)Kgamma has an important context-dependent role in neutrophil chemokinesis. Nat. Cell Biol. 2007; 9:86–91. [PubMed: 17173040]
33. Tang W, et al. A PLCβ/PI3Kγ-GSK3 Signaling Pathway Regulates Cofilin Phosphatase Slingshot2 and Neutrophil Polarization and Chemotaxis. Dev. Cell. 2011; 21:1038–1050. [PubMed: 22172670]

34. Miao Y, et al. Altering the threshold of an excitable signal transduction network changes cell migratory modes. Nat. Cell Biol. 2017; 19:329–340. [PubMed: 28346441]
35. Wilson K, et al. Mechanisms of leading edge protrusion in interstitial migration. Nat. Commun. 2013; 4:2896. [PubMed: 24305616]
36. Vargas P, et al. Innate control of actin nucleation determines two distinct migration behaviours in dendritic cells. Nat. Cell Biol. 2015; 18:43–53. [PubMed: 26641718]
37. Leithner A, et al. Diversified actin protrusions promote environmental exploration but are dispensable for locomotion of leukocytes. Nat. Cell Biol. 2016; 18:1253–1259. [PubMed: 27775702]
38. Yoo SK, et al. Differential Regulation of Protrusion and Polarity by PI(3)K during Neutrophil Motility in Live Zebrafish. Dev. Cell. 2010; 18:226–236. [PubMed: 20159593]
39. Sun H, et al. TIPE2 Controls Innate Immunity to RNA by Targeting the Phosphatidylinositol 3-Kinase-Rac Pathway. J. Immunol. 2012; 189:2768–2773. [PubMed: 22904303]
40. Sun J, Hilliard B, Xu L, Chen YH. Essential roles of the Fas-associated death domain in autoimmune encephalomyelitis. J. Immunol. 2005; 175:4783–4788. [PubMed: 16177127]
41. Xu L, et al. Arginase and autoimmune inflammation in the central nervous system. Immunology. 2003; 110:141–148. [PubMed: 12941151]
42. Ruan Q, et al. Development of Foxp3+ Regulatory T Cells Is Driven by the c-Rel Enhanceosome. Immunity. 2009; 31:932–940. [PubMed: 20064450]
43. Ruan Q, et al. The Th17 immune response is controlled by the Rel-RORγ-RORγT transcriptional axis. J. Exp. Med. 2011; 208:2321–2333. [PubMed: 22006976]
44. Wang T, Wei JJ, Sabatini DM, Lander ES. Genetic screens in human cells using the CRISPR-Cas9 system. Science. 2014; 343:80–84. [PubMed: 24336569]
45. Hirayama A, Adachi R, Otani S, Kasahara T, Suzuki K. Cofilin plays a critical role in IL-8-dependent chemotaxis of neutrophilic HL-60 cells through changes in phosphorylation. J. Leukoc. Biol. 2007; 81:720–728. [PubMed: 17130184]
46. Jo VE, Cambridge M. The Transwell Migration Assay. JoVE Sci. Educ. Database. 2016; :2–3. DOI: 10.3791/5644
47. Zhao H, Hakala M, Lappalainen P. ADF/Cofilin Binds Phosphoinositides in a Multivalent Manner to Act as a PtdIns(4,5)P_2-Density Sensor. Biophys. J. 2010; 98:2327–2336. [PubMed: 20483342]
48. Knight ZA, Feldman ME, Balla A, Balla T, Shokat KM. A membrane capture assay for lipid kinase activity. Nat. Protoc. 2007; 2:2459–2466. [PubMed: 17947987]

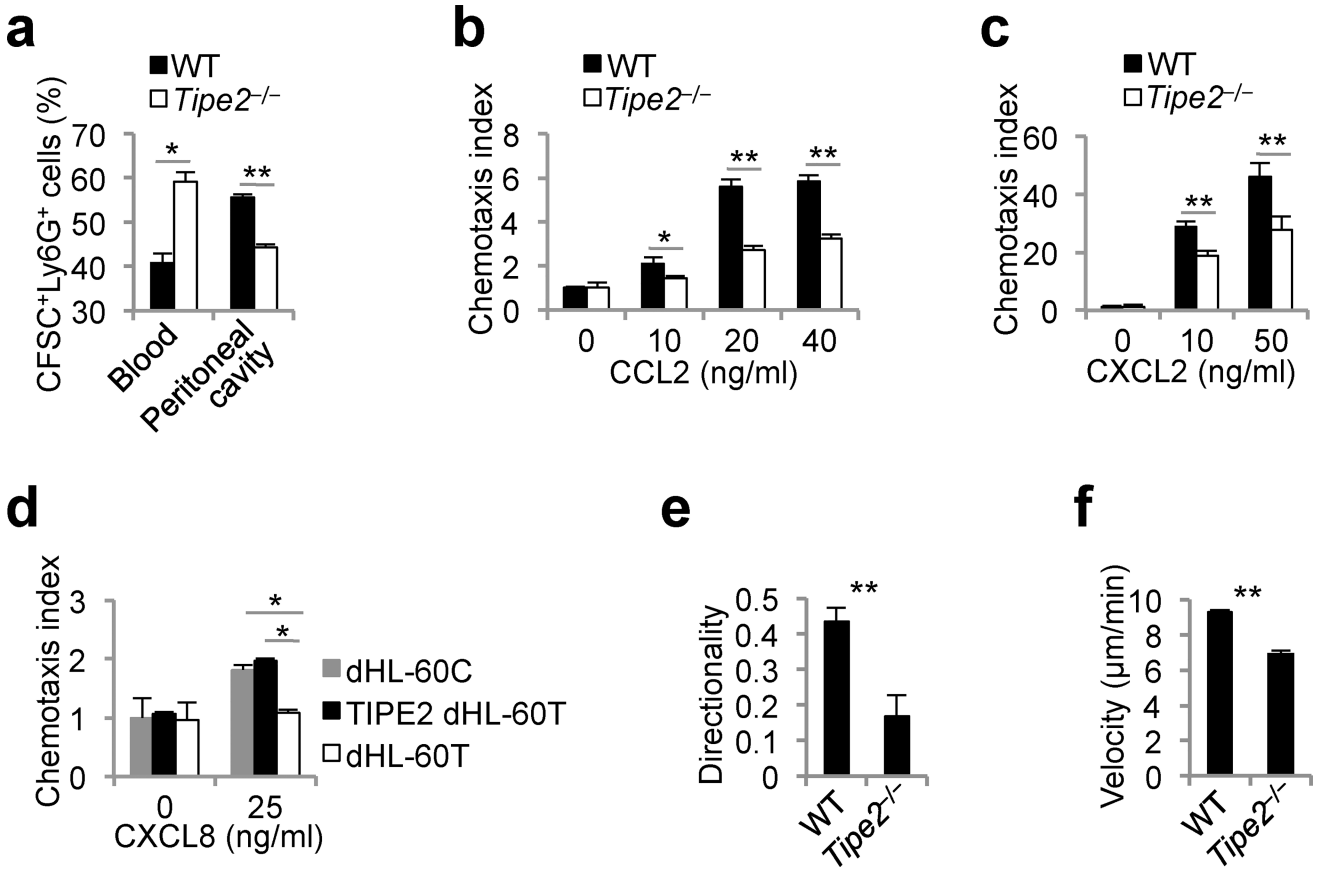

Figure 1. LY2940021. TIPE2 promotes leukocyte chemotaxis both *in vivo* and *in vitro*

(**a**) Wild-type (WT) mice with acute peritonitis were intravenously injected with CFSE-labeled *Tipe2*$^{-/-}$ CD45.2^{+} and WT CD45.1^{+} bone marrow cells mixed at 1:1 ratio. The percentages of injected WT and *Tipe2*$^{-/-}$ Ly6G^{+} cells in the blood and peritoneal cavity were determined 16 h later by flow cytometry. Values represent means ± SEM. The experiments were repeated two times with $n = 5$. (**b-d**) Chemotaxis indexes of WT and *Tipe2*$^{-/-}$ bone marrow-derived macrophages (b), WT and *Tipe2*$^{-/-}$ bone marrow neutrophils (c), or control dHL-60C, TIPE2-deficient dHL-60T, and TIPE2-expressing dHL-60T neutrophils (d) migrating through transwell filters toward CCL2, CXCL2 or CXCL8 as indicated. Values represent means ± SD. The experiments were performed in duplicates and repeated three times, n=6. (**e,f**) Directionality (**e**) and velocity (**f**) of WT and *Tipe2*$^{-/-}$ blood neutrophils migrating toward CXCL1 (200 ng/ml) on μ-slides were measured as described in Methods. The experiments were performed at least three times. The results of a representative experiment are shown, n ≥ 145. *DMI*, directional migration index. Values represent means ± SEM; *, $P < 0.05$; **, $P < 0.01$.

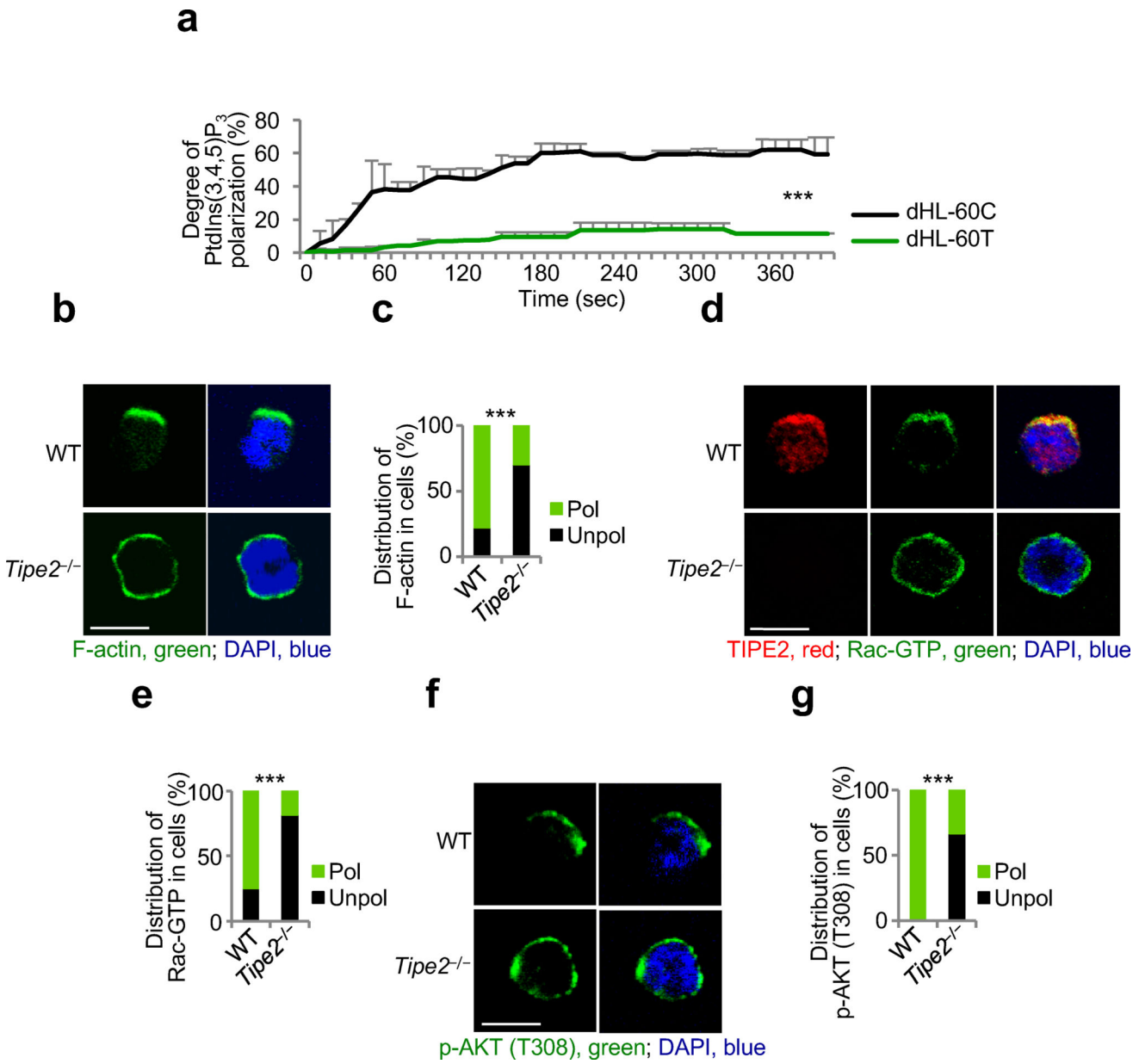

Figure 2. TIPE2 is required for chemoattractant-induced leukocyte polarization

(**a**) Time-lapse confocal microscopy for PtdIns(3,4,5)P_3 distribution in control dHL-60C and TIPE2-deficient dHL-60T neutrophils subjected to point-source stimulation with CXCL8 over the indicated times. The PtdIns(3,4,5)P_3 distribution was probed with eGFP-GRP1-PH domain; results are presented as degree of PtdIns(3,4,5)P_3 polarization. Values represent means ± SD. The experiments were repeated two times, n ≥ 45. (**b-g**) Confocal microscopy for the indicated molecules in wild-type (WT) and *Tipe2*$^{-/-}$ bone marrow neutrophils subjected to point-source stimulations with CXCL8. Panels b, d and f show representative images of each cell types (scale bars are 5 μm), whereas panels c, e, and g show the percentages of cells with polarized (*pol*) or unpolarized (*unpol*) distributions of the indicated molecules in each cell type. The experiments were repeated three times, n ≥ 30. ***, $P <$ 0.0001.

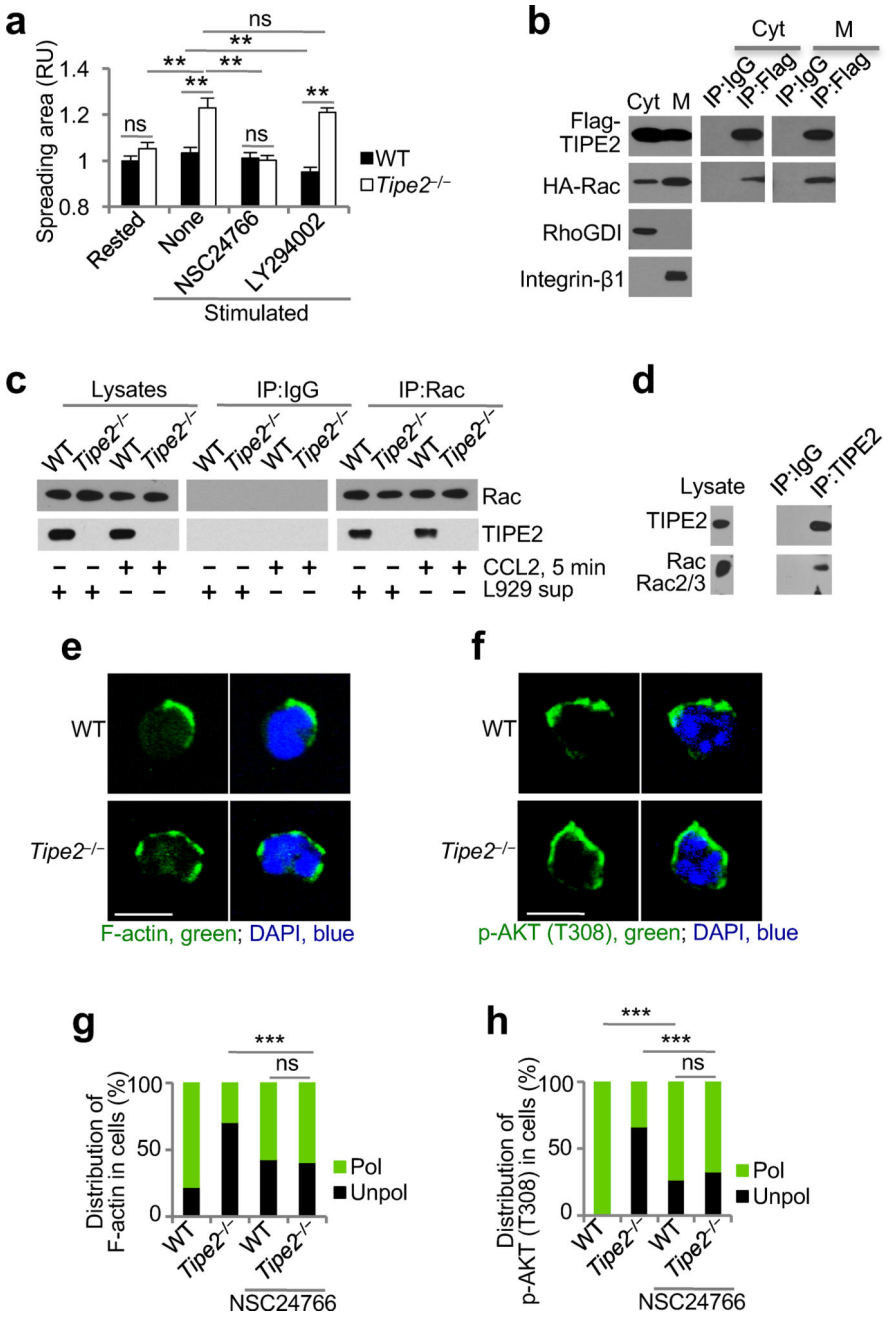

Figure 3. Rac-dependent functions of TIPE2 in chemotaxing cells

(**a**) Relative spreading areas of wild-type (WT) and *Tipe2*$^{-/-}$ bone marrow neutrophils, which were either rested or stimulated with CXCL8 from a point source (designated as stim), with or without pretreatments with Rac inhibitor (NSC24766) or PI(3)K inhibitor (LY294002). Values represent means ± SEM. The experiments were repeated at least two times, n ≥ 30. **, $P < 0.01$; ns, not significant; RU, relative units. (**b-d**) Co-immunoprecipitation (co-IP) analysis of TIPE2 interaction with Rac. The experiments were performed at least three times. The results of a representative experiments are shown. (**b**) Cytoplasmic (Cyt) and membrane (M) protein fractions of 293T cells expressing

recombinant Flag-TIPE2 and HA-Rac proteins were subjected to co-IP with anti-Flag or control IgG. (**c**) Lysates of WT and *Tipe2*$^{-/-}$ BMDMs cultured with or without L929 cell supernatant (designated as L929 sup) or CCL2 (stimulated for 5 min) were subjected to co-IP with anti-Rac or control IgG. (**d**) Lysates of dHL-60T cells were subjected to co-IP with anti-TIPE2 or control IgG. The precipitates were analyzed by immunoblot for the indicated proteins. (**e-h**) The subcellular distributions of F-actin (**e,g**) and pAKT(308) (**f,h**) in WT and *Tipe2*$^{-/-}$ bone marrow neutrophils pretreated with Rac inhibitor and stimulated with CXCL8 (point source) were determined by confocal microscopy. Panels e and f show representative images of each cell types (scale bars are 5 μm), whereas panels g and h show the percentages of cells with polarized (pol) or unpolarized (unpol) distributions of the indicated molecules in each cell type. e-h, The experiments were repeated three times; g and h, n ≥ 30. ***, $P < 0.0001$; *ns*, not significant.

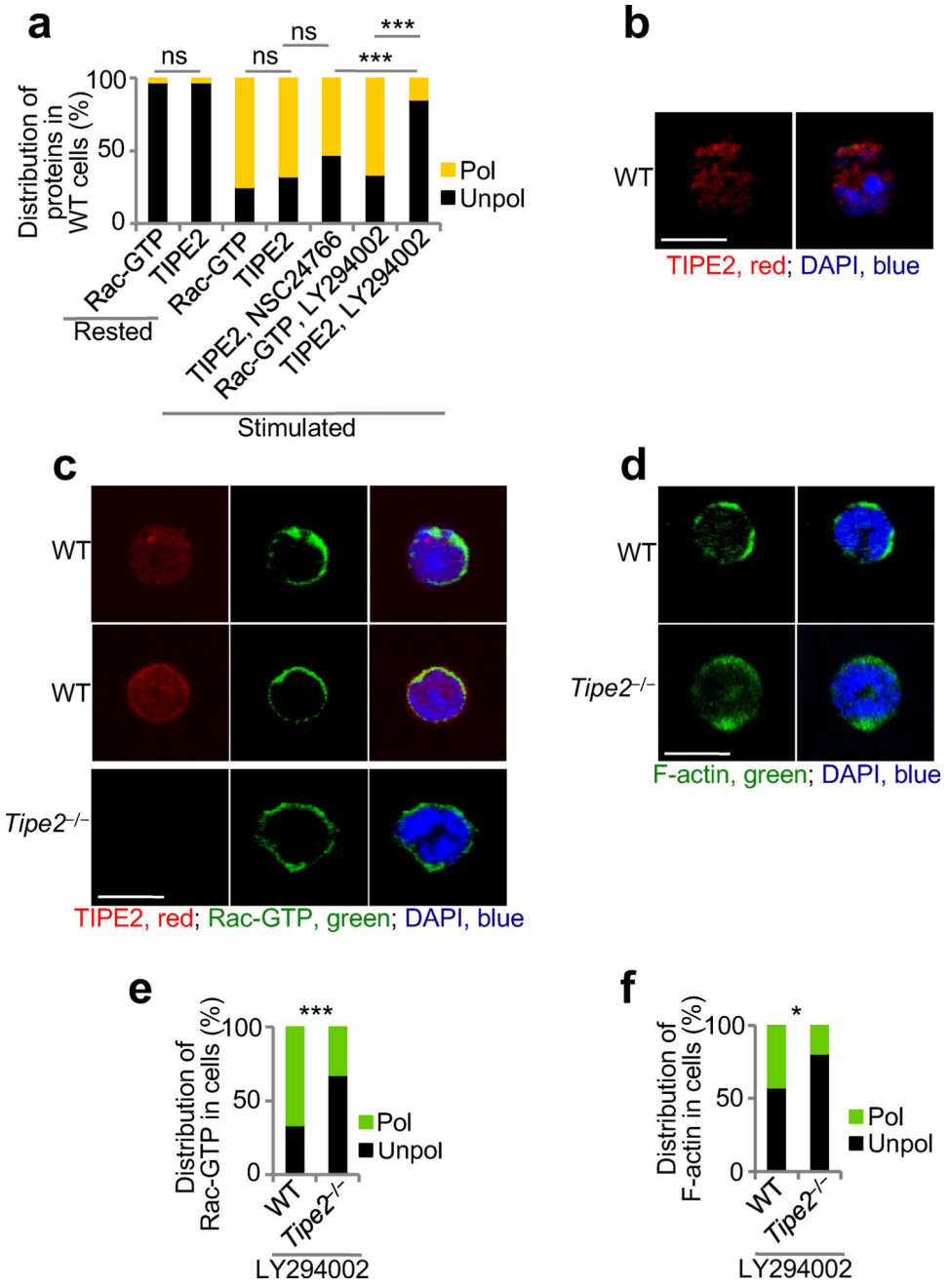

Figure 4. Rac-independent functions of TIPE2 in chemotaxing cells

(**a-f**) Confocal microscopy for subcellular distribution of TIPE2 (**a-c**), Rac-GTP (**a,c,e**) and F-actin (**d,f**) in wild-type (WT) and *Tipe2*$^{-/-}$ bone marrow neutrophils, which were rested or stimulated with CXCL8 (point source), with or without pretreatments with Rac inhibitor (NSC24766) (**a,b**) or PI(3)K inhibitor (LY294002) (**a,c-f**). Panels a, e and f show the percentages of cells with polarized (pol) or unpolarized (unpol) distributions of the indicated molecules, whereas panels b-d show representative images (scale bars are 5 μm). ns, not significant. The experiments were repeated at least two times; a, e-f, n ≥ 30. *, $P < 0.05$; ***, $P < 0.001$; *ns*, not significant.

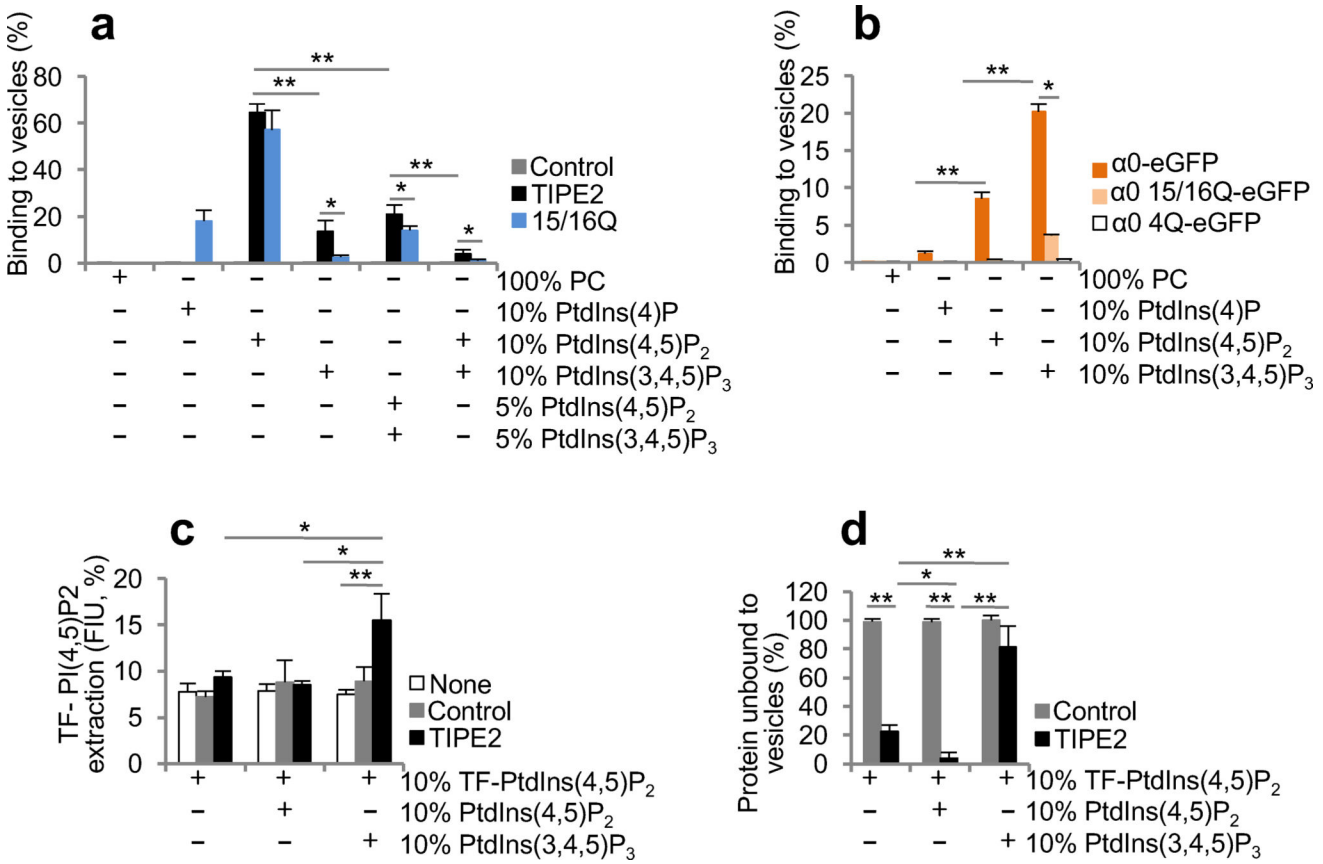

Figure 5. TIPE2 functions as a PtdIns(4,5)P_2 transfer protein in PtdIns(3,4,5)P_3-enriched lipid bilayers

(**a,b**) The percentages of TIPE2, 15/16Q, and control protein (**a**), or α0-eGFP, α0 15/16Q-eGFP, and α0 4Q-eGFP (wild-type or lysine-mutated TIPE2 α0 helixes fused with eGFP) (**b**) bound to small unilamellar vesicles (SUV) containing the indicated lipids, as determined in the phosphoinositide binding assay. (**c**) The percentages of TopFluor (TF)-PtdIns(4,5)P_2 extracted from SUV containing the indicated lipids by TIPE2 or control protein, as determined in the phosphoinositide extraction assay. FIU, fluorescence intensity units. (**d**) The percentages of TIPE2 or control protein remained unbound to SUV containing the indicated lipids, as determined in the phosphoinositide extraction assay. Values represent means ± SD. *, $P < 0.05$; **, $P < 0.01$; the experiments were repeated at least three times (n ≥ 3).

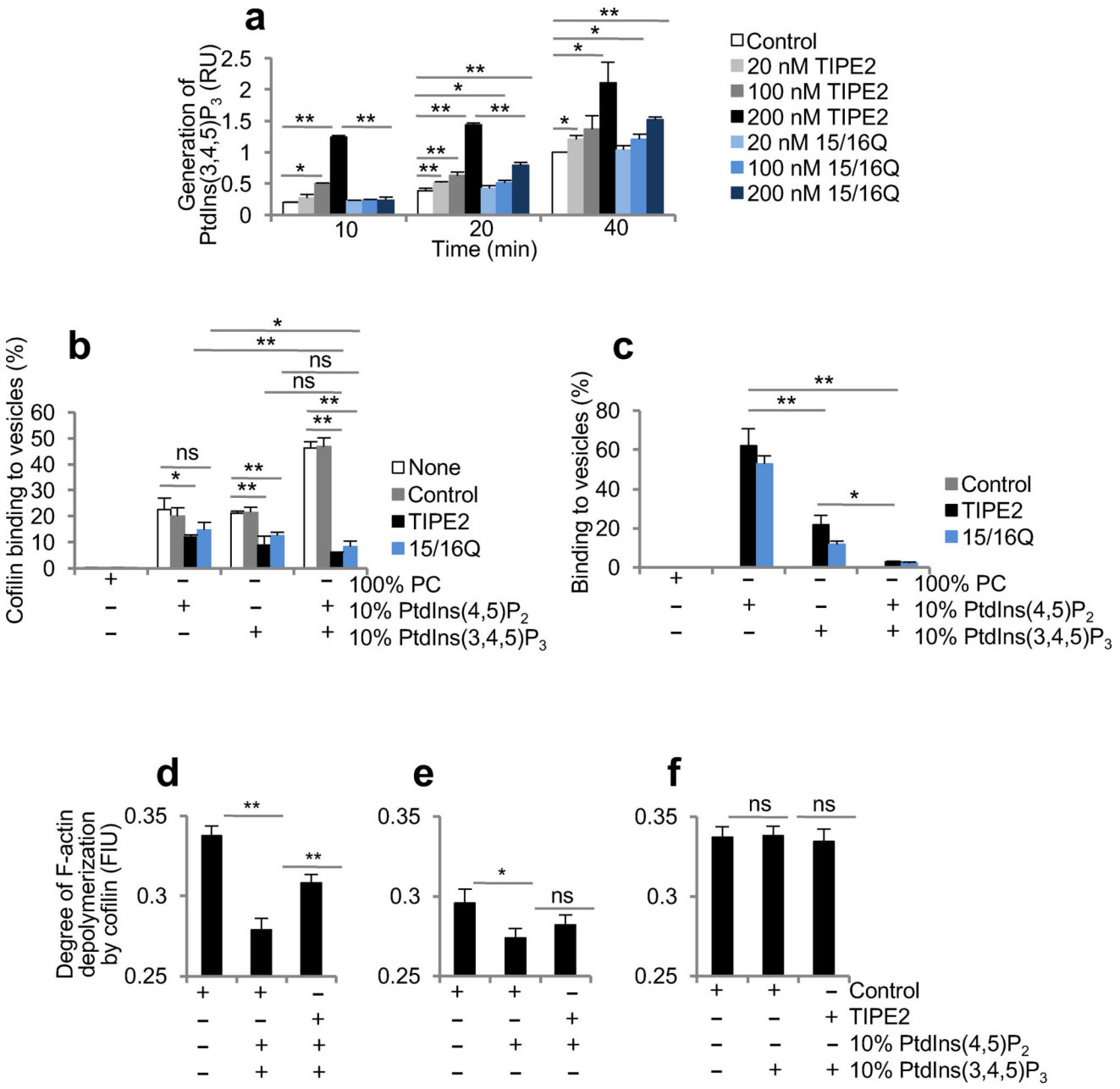

Figure 6. TIPE2 controls phosphoinositide signaling through PtdIns(3,4,5)P_3-dependent mechanisms

(**a**) Time course of PI(3)K-catalyzed generation of PtdIns(3,4,5)P_3 in the absence or presence of TIPE2 or 15/16Q at the indicated concentrations. RU, relative units. (**b**) Percentages of cofilin bound to small unilamellar vesicles (SUV) containing the indicated lipids in the absence or presence of TIPE2, 15/16Q, or control protein, as determined in the phosphoinositide binding assay. (**c**) The percentages of TIPE2, 15/16Q, or control protein bound SUV, as determined in the phosphoinositide binding assay of cofilin. (**d-f**) The degree of cofilin-dependent F-actin depolymerization in the presence of control protein, control protein plus SUV, or TIPE2 plus SUV was analyzed as described in Methods. *FIU*,

fluorescence intensity units. For panels a, b and c, values represent means ± SD. For panels d-f, values represent means ± SEM. *, $P < 0.05$; **, $P < 0.01$; *ns*, not significant; the experiments were repeated at least three times ($n \geq 3$).

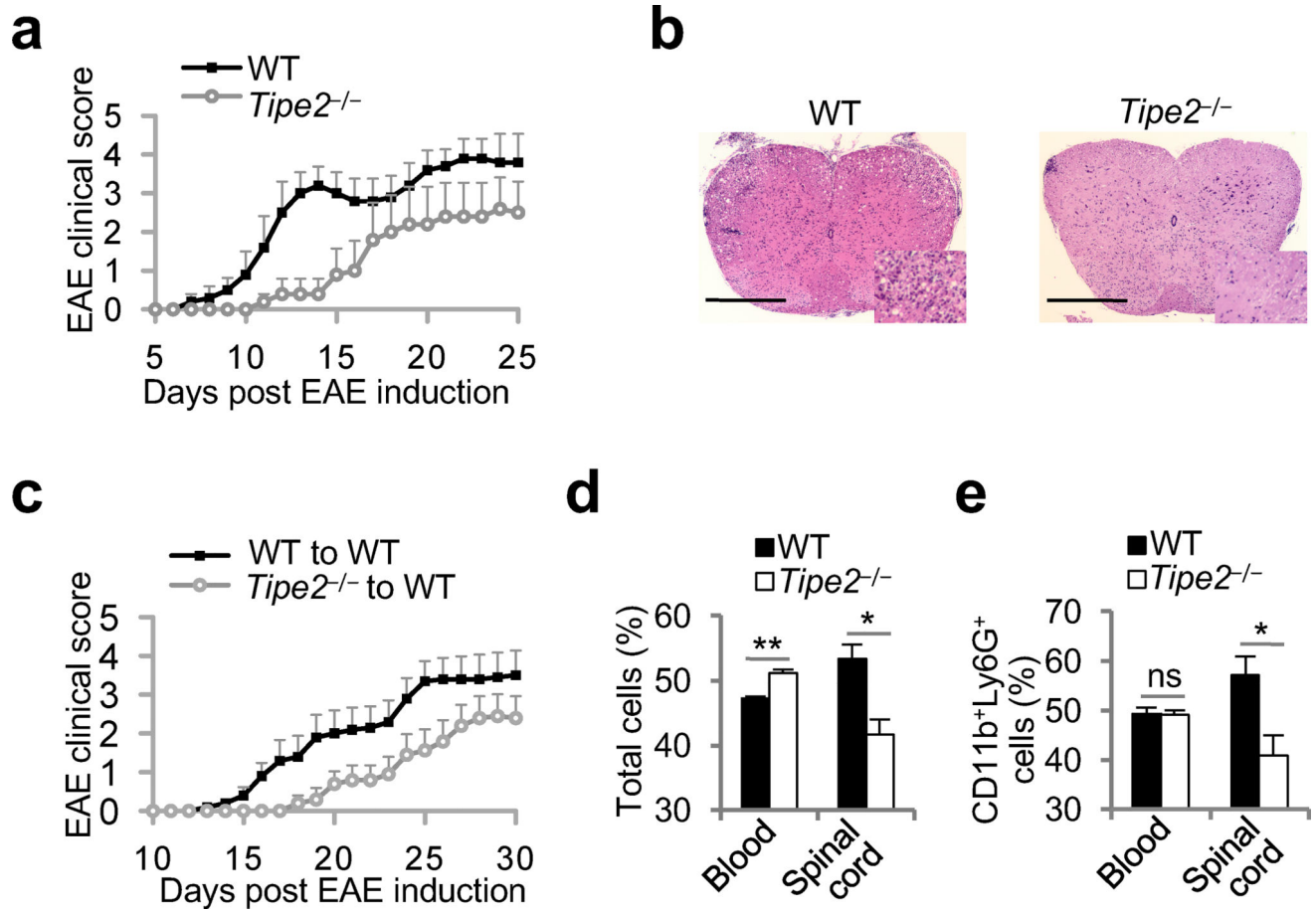

Figure 7. Reduced encephalomyelitis and leukocyte infiltration in the nervous tissue of *Tipe2*$^{-/-}$ mice

(**a**) *Tipe2*$^{-/-}$ and wild-type (WT) mice were immunized with myelin oligodendrocyte glycoprotein (MOG) peptide to induce experimental autoimmune encephalomyelitis (EAE), and the clinical scores of the disease were recorded daily. The experiments were repeated three times, $n = 8$; $P < 0.0001$ for differences after day 10. (**b**) Twenty-five days after immunization, *Tipe2*$^{-/-}$ and WT mice were sacrificed, and their spinal cords collected, sectioned, and stained with hematoxylin and eosin. The experiments were repeated three times, $n = 8$; representative images of the spinal cord sections are shown; scale bars are 500 μm. (**c**) WT mice were sub-lethally irradiated, and injected intravenously with either *Tipe2*$^{-/-}$ or WT bone marrow cells. Seven weeks later, mice were immunized with MOG to induce EAE, and the clinical scores of the disease were recorded daily. The experiments were repeated three times, $n = 10$. $P = 0.0005$ for differences after day 16. (**d,e**) WT mice were sub-lethally irradiated, and injected with mixed WT and *Tipe2*$^{-/-}$ bone marrow cells (at a ratio of 1:1). Seven weeks later, mice were immunized with MOG peptide to induce EAE, and sacrificed on the day of the disease onset. The percentages of WT and *Tipe2*$^{-/-}$ leukocytes (*Total cells*) and CD11b^{+}Ly6G^{+} cells in the blood and spinal cord leukocyte preparations were determined by flow cytometry. The experiments were repeated two times, $n = 3$. For panels a, c, d and e, values represent means ± SEM; *, $P < 0.05$; **, $P < 0.01$.